Controlling Sound Wave Propagation in Topological Crystalline Insulators and Rainbow-Trapping

An-Yang Guan,[1,†] Zhang-Zhao Yang,[1,†] Wen-Jie Yang,[1] Shi-Feng Li,[1] Xin-Ye Zou,[1,2,*] and Jian-Chun Cheng[1,2]

[1]*Key Laboratory of Modern Acoustics, MOE, Institute of Acoustics, Department of Physics, Collaborative Innovation Center of Advanced Microstructures, Nanjing University, Nanjing 210093, People's Republic of China*
[2]*State Key Laboratory of Acoustics, Chinese Academy of Sciences, Beijing 100190, People's Republic of China*

Topological crystalline insulators (TCIs) capable of supporting topological states protected by spatial symmetries have given rise to a promising platform for wave manipulation due to their robustness. Unfortunately, the methods to control the group velocity of topological states in classical wave systems are rarely discussed, which is an important issue in practical applications. In this work, we propose a method to change the frequency and propagation speed of topological edge states through on-site potential and realize a prototype of topological rainbow concentrator in a resonant acoustic system at subwavelength, which can separate different frequency components of propagating sound waves. The concepts of classical wave systems are combined with condensed matter physics, and the rigorous correspondence of TCIs and their analogs in acoustic resonant systems is demonstrated to design topological acoustic devices. Further, the implementation of controlling the group velocity of topological states precisely in a two-dimensional Su-Schrieffer-Heeger model is presented in detail, which can be extended to other TCI models and higher dimensions. We hope this work will enlarge possible applications of topological phenomena and the manufacture of acoustic devices.

I. INTRODUCTION

Originating from condensed matter physics, topological phases of matter that support robust one-way edge states have rendered possibilities for dissipationless wave manipulation in classical wave systems [1–6]. More recently, the concept of topological crystalline insulators (TCIs) supporting higher-order topological states has greatly broadened the material search for classes of topological insulators [7–12]. Distinct from conventional topological insulators, the topological phases of TCIs are protected by certain spatial symmetries of the bulk lattice and originate from the boundary-induced filling anomaly of fractional charges [13,14]. So far, TCIs have been successfully implemented in optics [15–21], mechanics [22,23], microwaves [24], circuits [25,26], and acoustics [27–36].

For the class of spinless and time-reversal invariant topological crystalline insulators, the topological states characterized by bulk polarization are relatively easier to implement in classical wave systems, which naturally provide an ideal platform to trap the wave with specific energy (frequency) robustly at the boundaries or the corners of the structure. However, although a lot of careful researches demonstrate the topological states in TCIs theoretically or experimentally, the propagation properties such as the group velocity of the topological state are rarely discussed, which is an important problem in practical applications of TCIs. An example is utilizing topological states to implement rainbow-trapping. Rainbow-trapping, which separates and traps waves with different frequencies at different spatial positions, has been presented in electromagnetic wave systems [37–47], acoustic systems [48–50], and mechanical systems [51–56]. In these works, researchers use various methods to control the dispersion relationship of waves in different systems, so that waves can be localized at different locations in space. Some recent works have implemented rainbow-trapping in topological states [57–62]. The in-gap mode is slowed without reducing the bulk band gap, which remains protected against strong disorder. However, existing methods often require an additional region or changes to the lattice in bulk. From an application point of view, a method that can directly control the propagation velocity of topological states at the boundary is needed.

The purpose of this work is to present a method of controlling the propagation velocity of sound waves in

---

*xyzou@nju.edu.cn
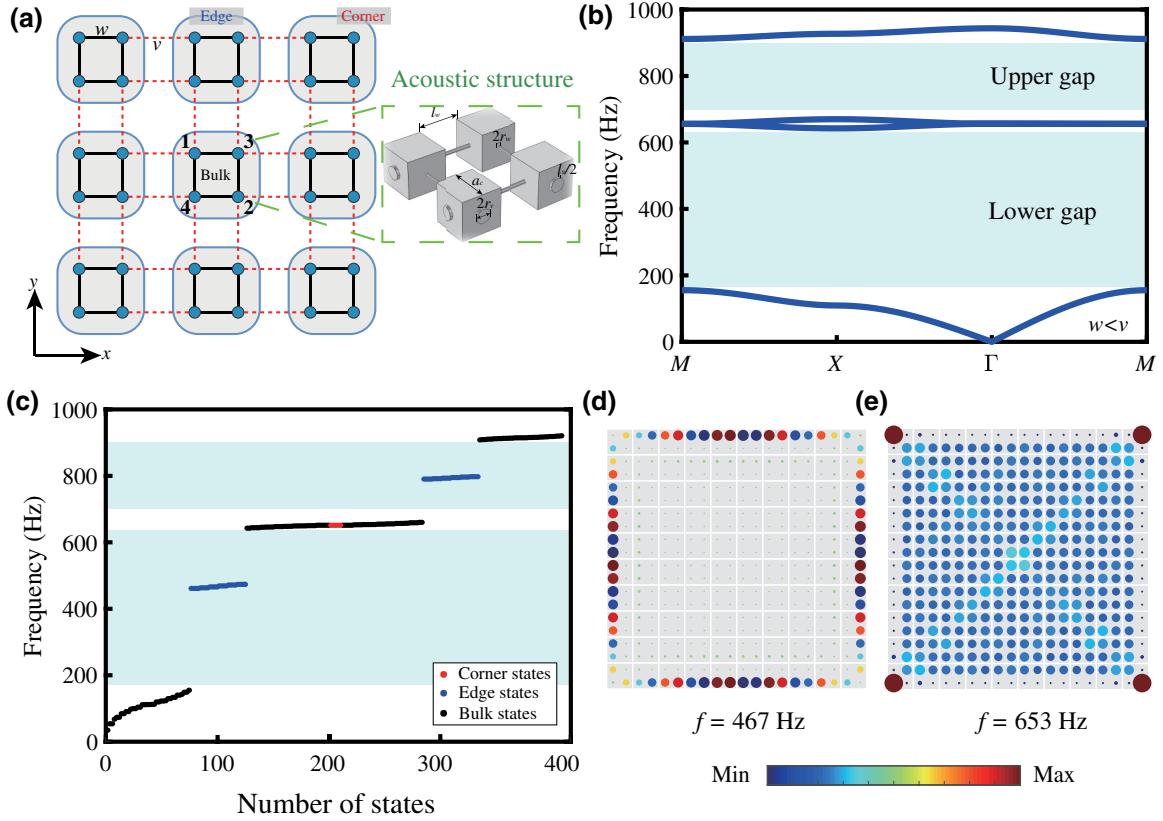†These authors have contributed equally to this work.

FIG. 1. (a) Schematic of the 2D SSH model. (b) Energy spectrum of the periodic structure. (c) Energy spectrum of the finite structure. (d) The boundary-localized state isolated in the lower gap. (e) The "zero-energy" corner-localized state degenerate with bulk states.

the topological states of TCIs at different frequencies in order to achieve acoustic rainbow-trapping. Based on a two-dimensional (2D) Su-Schrieffer-Heeger (SSH) model, we demonstrate the rigorous correspondence between the impedance of classical wave systems and the hopping and on-site terms of tight-binding models, which reveals that instead of adding deformation to the bulk, the frequencies and the group velocities of edge states can be precisely and independently controlled by merely tuning the surface impedances of metamaterials. This feature naturally provides a promising platform for topologically protected wave trapping, and a prototype of a subwavelength topological rainbow concentrator is experimentally presented. In particular, we show that the trivial environment is not actually required, which reduces the volume of the entire structure.

II. THE ACOUSTIC TOPOLOGICAL CRYSTALLINE INSULATOR AND ITS ON-SITE POTENTIAL

We focus on linear classical wave systems and start with a typical 2D SSH model as depicted in Fig. 1(a). The inset shows the corresponding acoustic structure, which simulates atoms with cavities and hoppings with tubes.

Figure 1(b) shows its band structure for the parameters $a_c = 30$ mm, $l_w = 120$ mm, $l_v = 20$ mm, $r_w = 1.5$ mm, and $r_v = 4$ mm. Here, the intra- and interlattice inductances connecting the cavities are defined as L_w and L_v, while the capacitance of the cavities is C, which can be obtained according to the geometrical parameters of the structure. ω is the angular frequency of the Bloch wave function. For the bulk lattice, the wave equation in the form of the Schrödinger equation in the momentum space can be written as

$$\hat{\mathscr{H}}_k \Psi_k = \omega^2 \Psi_k, \tag{1}$$

where $\Psi_k = [\psi_1, \psi_2, \psi_3, \psi_4]^T$ is the Bloch wave function in the bulk lattice and

$$\hat{\mathscr{H}}_k = -(2w + 2v)\mathbb{I}_{4\times4} + \mathscr{H}, \tag{2}$$

where w and v are the intra- and interlattice hopping terms, respectively, and $\mathbb{I}_{4\times4}$ is the unitary matrix. $\mathscr{H}$ is a Hermitian matrix where $\mathscr{H}_{13} = \mathscr{H}_{24}^* = w + ve^{ik_x}$ and $\mathscr{H}_{14} = \mathscr{H}_{23}^* = w + ve^{-ik_y}$, and the others are zero components. In the present model, the rigorous correspondence between the hopping terms and the impedances can be directly obtained as $w = -1/L_w C$ and $v = -1/L_v C$. Here
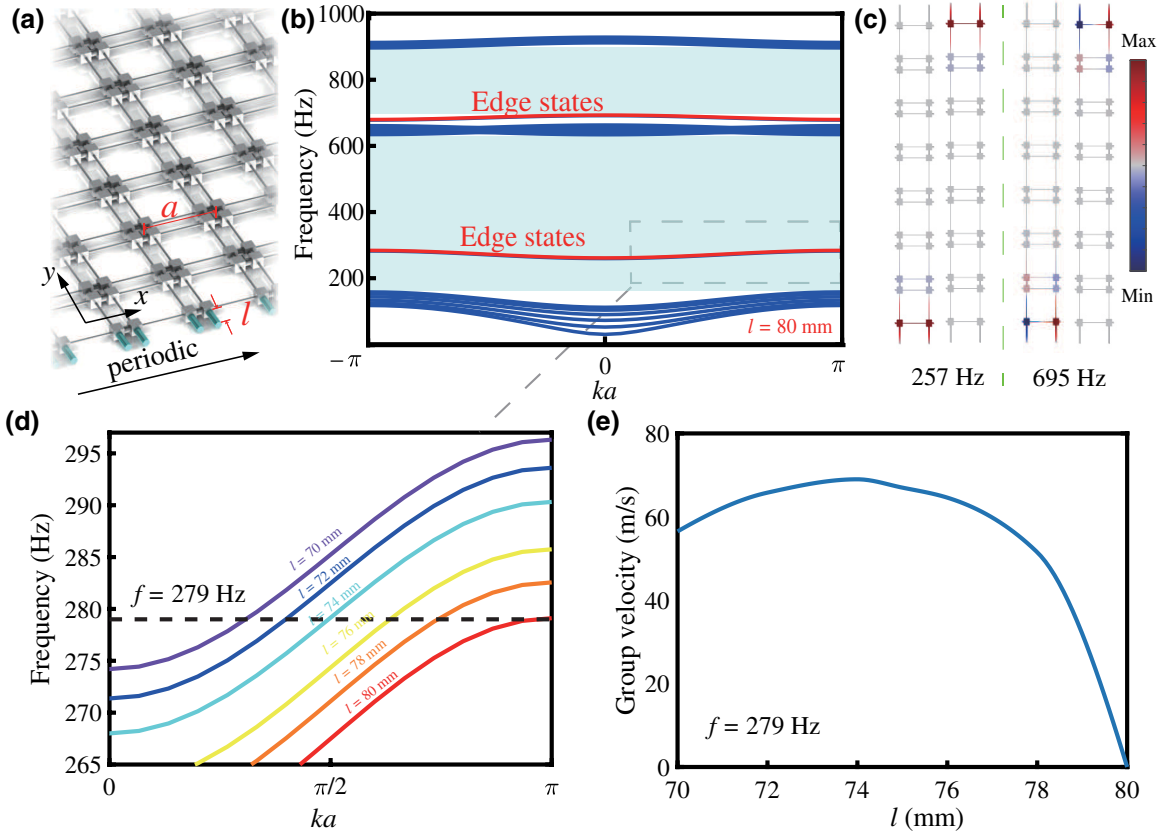
FIG. 2. (a) The ribbon structure truncated in the y direction and periodic in the x direction. The outermost tubes are marked in blue. (b) Energy spectrum of the ribbon structure. (c) Sound pressure field distribution of topological edge states when $ka = 0$. (d) The spectrum of edge states with different l of the ribbon structure. (e) The group velocity of the edge state at 279 Hz as a function of l.

$w = -2.51 \times 10^5$ Hz^2 and $v = -8.17 \times 10^6$ Hz^2 (see Supplemental Material [63]).

The higher-order topology of the nth band protected by C_4 symmetry can still be characterized by the dipole moments $\mathscr{P}^{(n)} = (\mathscr{P}_x^{(n)}, \mathscr{P}_y^{(n)})$, where [64]

$$\mathscr{P}_j^{(n)} = -\left(\frac{1}{2\pi}\right)^2 \int_{1BZ} \text{Tr}[\mathscr{A}_{j,k}] d^2 k, \quad (3)$$

where $[\mathscr{A}_{j,k}]^{p,q} = -i\langle \psi_k^p | \partial_{k_j} | \psi_k^q \rangle$ ($j = x, y$) is the non-Abelian Berry connection, p and q running over the occupied bands. The "$1BZ$" represents the first Brillouin zone. In addition, a corner-induced topological quadrupole index can also be defined as [65]

$$\mathcal{Q}_{xy} = \sum_{n=1}^{occ} \mathscr{P}_x^{(n)} \mathscr{P}_y^{(n)}. \quad (4)$$

For two occupied bands condition, $\mathscr{P}_x^{(1)} = \mathscr{P}_y^{(1)} = \mathcal{Q}_{xy} = 0.5$ when $v > w$ indicates that the topological edge states and corner states are predicted to emerge at the boundaries and corners of a finite structure with open boundaries, as shown in Figs. 1(c)–1(e).

One intrinsic consideration of the theoretical models is that chiral symmetry is perfectly preserved even if in the open-boundary condition, and therefore boundary-localized modes are predicted to be pinned to zero energy (midgap); even in much of the experimental studies, on-site potential is always considered independent. Nevertheless, as demonstrated in Eq. (2), the on-site potential is strongly coupled with the hopping terms in real physical systems. Therefore, for a finite structure, if without rigorous compensations in the boundary lattices, chiral symmetry breaking of the corresponding lattices will inevitably result in the shift of the on-site potential [12]. For example, for a C_4-symmetric acoustic system with absolute hard-wall boundary condition or optical system with perfect magnetic conductorlike boundary condition, the surface impedance being $Z = \infty$ yields these terms in the boundary lattices to be $\varepsilon^{\text{edge}} = -2w - v$, while the on-site potential of the atoms in the corner lattices is $\varepsilon^{\text{corner}} = -2w$. What is more, under the same conditions, the lengths of the outermost tubes directly determine their impedance. In the Supplemental Material, we deduce the mathematical relationship between the two [63]. From this point of view, we can change the length of the tube at the corresponding
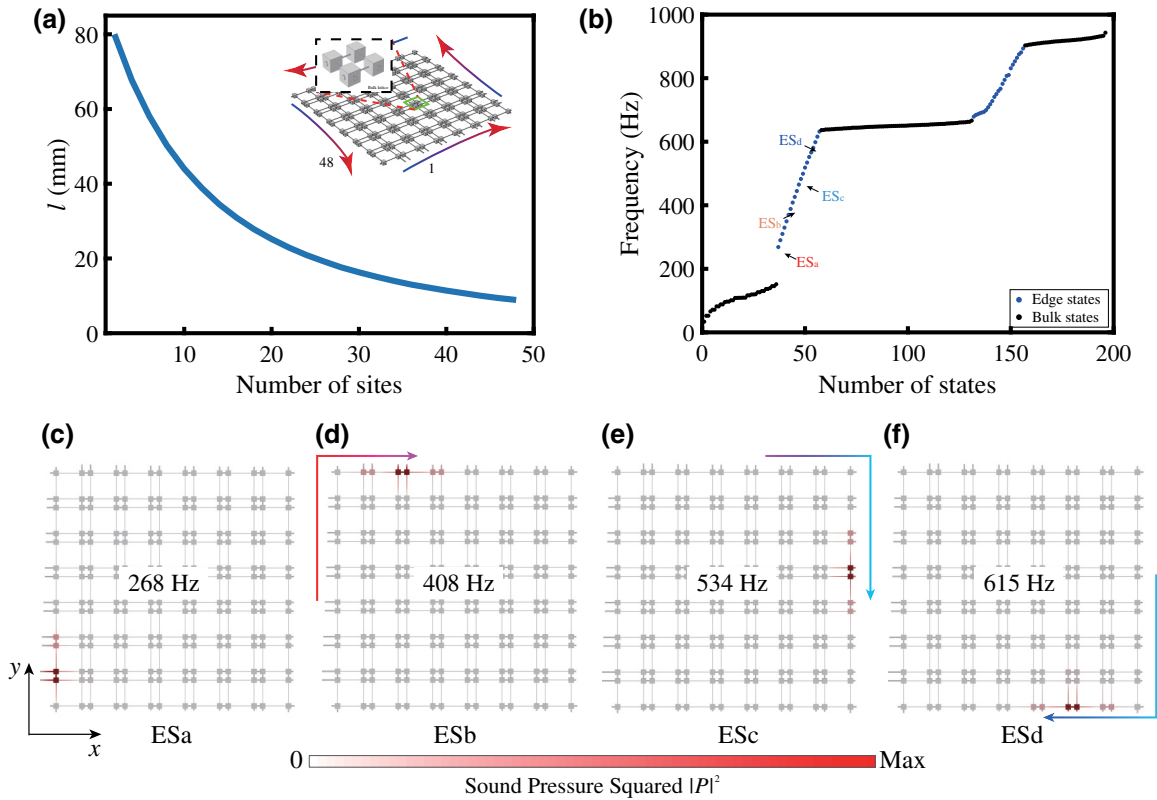
FIG. 3. (a) The lengths of the outermost tubes l vary with their sites in a 7×7 structure. (b) Eigenfrequency spectrum of the rainbow concentrator. Movement of the boundary-localized states with frequencies of (c) 268 Hz, (d) 408 Hz, (e) 534 Hz, and (f) 615 Hz.

position in the acoustic model to change the on-site potential of a certain position.

III. CHANGE THE GROUP VELOCITY OF TOPOLOGICAL EDGE STATE

Crucially, we argue that the intrinsic chiral symmetry breaking is the key to shift the frequencies of the topological states and change their group velocities. Although the emergence of the topological states is determined by the bulk topology, due to the natural property of the edge states and corner states that these states trapped within the boundary lattices exponentially attenuate into the bulk, the energy (frequency) of the topological states mainly depends on the on-site potential of the surface atoms in the boundary lattices; namely, the topological states and the trivial bulk states are independent of each other, even if they can be degenerate. As a result, this particular feature indicates that, by controlling the on-site potential, i.e., the surface impedances in the classical wave systems, of the boundary lattices, the frequencies of the edge states and corner states can be shifted precisely and freely.

To explain this, based on the theoretical model discussed above, we construct a ribbon structure truncated in the x direction and periodic in the y direction with the unit cell in Fig. 2(a). We deliberately add additional on-site

potential to the up-and-down boundaries by changing the lengths l of the outermost tubes as shown in Fig. 2(a). The nontrivial properties of the bulk lattice determine that there will be gapless edge states on the upper and lower boundaries as shown in Fig. 2(b). The sound pressure field distribution of topological edge states in the two gaps is shown in Fig. 2(c). However, the differences in on-site potential at the boundaries cause their frequencies to shift. Correspondingly, the frequencies of the edge states in the first gap with different l are presented in Fig. 2(d). It is clear to see that the edge states will always exist in the first gap, but their frequencies will shift with l. Analogous to condensed matter physics, this acoustic phenomenon arises from the effect of on-site potential on topological states, which is clearly demonstrated in the Supplemental Material through the analytical solution of topological states in a 1D SSH model [63]. This result also indicates that the topologically trivial environment is not essential.

In this way, the edge states can be tuned precisely to trap the waves with specific frequencies without impacting the bulk topology. Such property indicates the promising application of TCIs as topologically protected frequency concentrators. In fact, the energy band in Fig. 2(d) is the dispersion relation of the edge state, from which we can calculate the group velocities c_g of the edge state
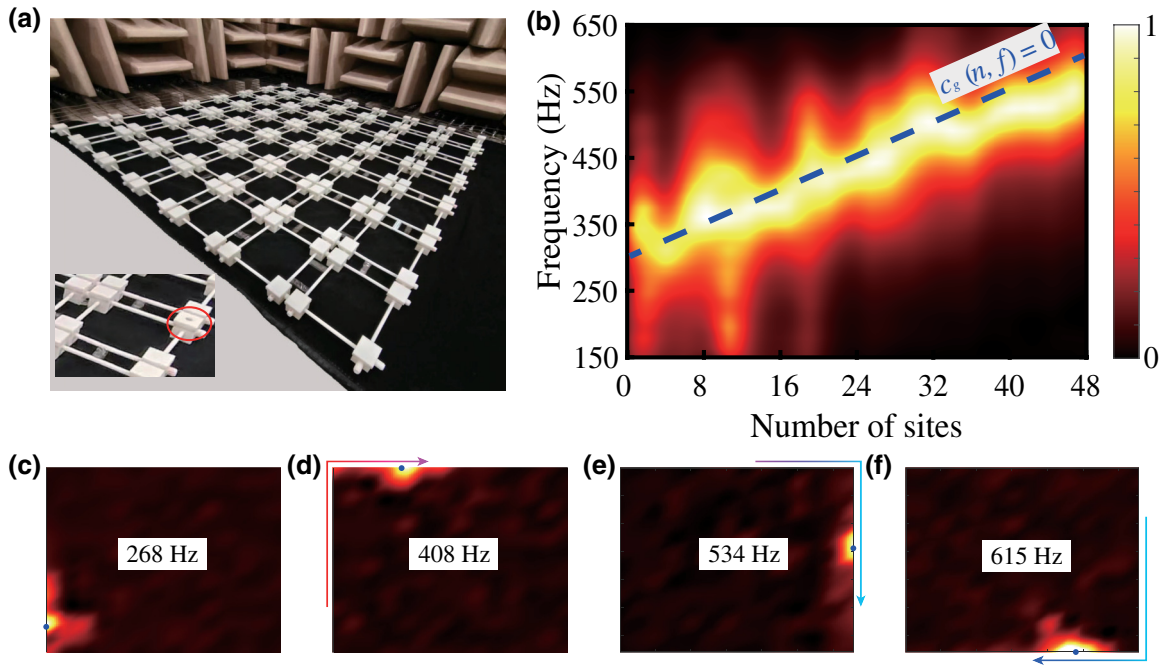
FIG. 4. (a) Schematic of the experimental sample. The inset shows the hole in which to place the speaker or microphone. (b) The measured intensity spectra of different sites. The results of the sound field at (c) 268 Hz, (d) 408 Hz, (e) 534 Hz, and (f) 615 Hz. The blue dots are the locations of sound sources.

through $c_g = d\omega/dk$. For example, Fig. 2(e) shows the group velocity of the edge state at 279 Hz as a function of l. It is worth noting that when l approaches 80 mm at 279 Hz, the group velocity gradually tends to 0. In this case, the sound wave is in a stationary state, which means that the energy of the sound wave is localized in a certain position. At different frequencies, the group velocity $c_g = 0$ corresponds to different l. This provides a theoretical basis for us to achieve the separation of different frequencies in an acoustic rainbow. Another essential feature of the 2D SSH model is that the nontrivial topology exists only when $v/w > 1$. When $|v|$ is much larger than $|w|$, the gaps are wider and the edge states exponentially attenuate into the bulk faster; crucially, the coupling oscillations of the atoms within the lattices can be approximately neglected. Therefore, for large v/w, the shift of the on-site potential of the paired interlattice atoms would hardly affect the other pairs, which implies that the topological states trapped within the corresponding lattices can be tuned independently (see Supplemental Material [63]).

IV. THE IMPLEMENTATION OF TOPOLOGICAL RAINBOW-TRAPPING

Rainbow-trapping, which refers to separate different frequency components of a wave at different spatial positions, is designed by controlling the dispersion in composite materials. Recently, interesting research achieved a topological rainbow concentrator of photonic crystals using synthetic dimensions in scattering-type photonic crystals [59]. By comparison, in our design the acoustic TCIs are based on resonant systems, which allow size of the structures to be much smaller than the wavelength. Further, our model strictly corresponds to the discrete 2D SSH model, which makes the process more convenient. We can determine the parameters in the Hamiltonian such as hopping and on-site potential according to the required frequency range. Then, according to these parameters in theoretical models, the impedances of the required acoustic structures can be calculated, and finally the geometric size of the actual sample such as the volumes of the cavities and the lengths and radii of the tubes can be determined.

We construct a finite 7×7 structure, in which the lengths of the outermost tubes vary with their sites as shown in Fig. 3(a), to demonstrate the ability to dwell sound waves at a specific frequency in the gap. The eigenfrequencies of this structure are shown in Fig. 3(b). It can be seen that a series of edge states appear in the forbidden band from 150 to 620 Hz. In our design, the location where the sound waves stop varies with frequencies, as shown in Figs. 3(c)–3(f). As illustrated in Fig. 4(a), we make a sample with 3D-printing technology to confirm this point. In order to place the sound source or measure the sound field at a certain position, the cavity at the corresponding position is perforated in which to place the speaker or microphone. The sound source is placed at different positions on the boundary, and the frequency response at
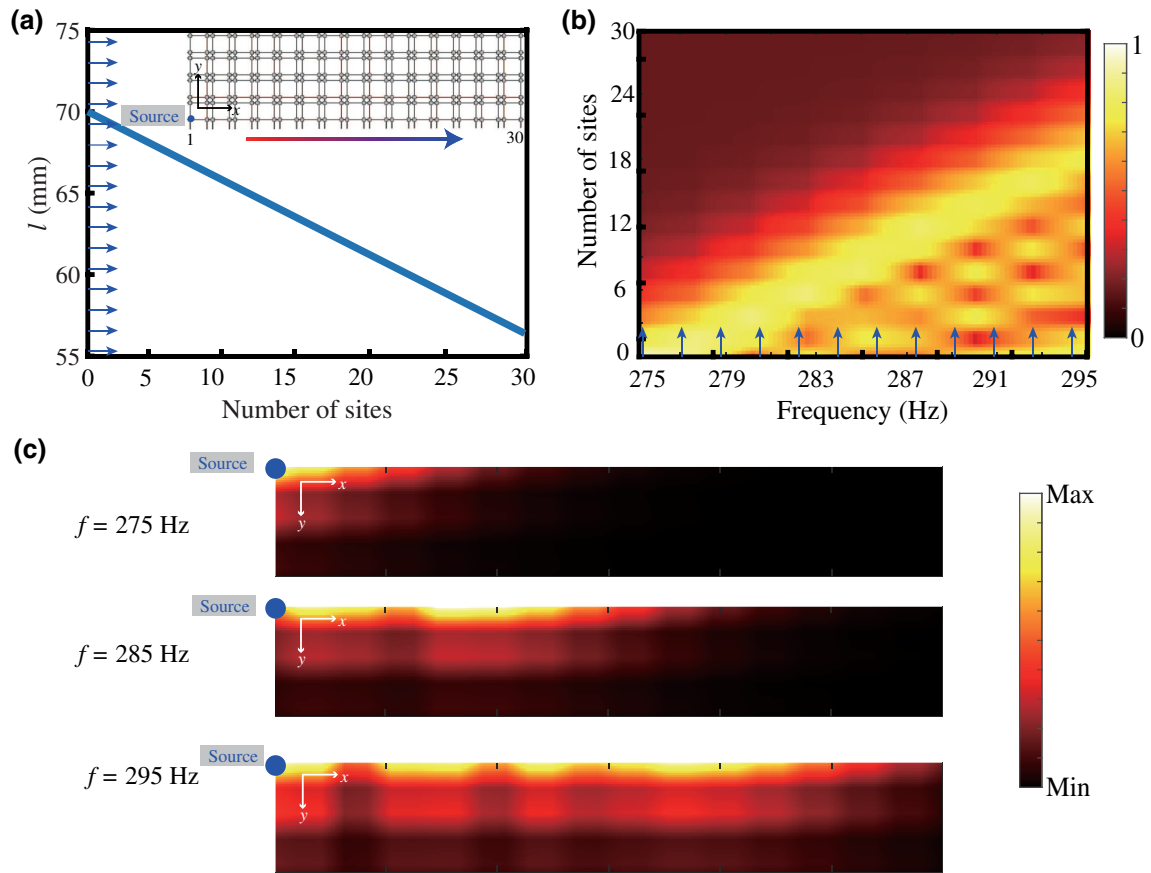
FIG. 5. (a) The lengths of the outermost tubes *l* vary with their sites. The sound source is placed in the cavity at site 1. The inset shows the experimental configuration. (b) The propagation of sound waves of different frequencies. (c) Sound pressure field map at different frequencies.

the adjacent cavity is measured by sweeping the frequency. Figure 4(b) shows the measured intensity spectra of different sites. For a certain position, if the group velocity of the sound wave is zero at a certain frequency, then the energy of the sound wave is localized at that position. Thus, a peak of intensity occurs at that site and at that frequency. The peak of energy intensity moves with frequency *f* and site number *n* and then forms the bright strip in Fig. 4(b). This strip should be consistent with the curve formed by all points (n, f) in Fig. 4(b) satisfying $c_g(n, f) = 0$, where c_g is regarded as a function of frequency *f* and site number *n*. The curve satisfying $c_g(n, f) = 0$ also can be obtained from the simulation results in Fig. 3. In the simulation calculation for solving the eigenmode, each eigenmode corresponds to a frequency *f* and a site number *n* where the sound energy density is the largest, and these points (n, f) form the blue line in Fig. 4(b). This line is in the bright strip in Fig. 4(b), which is consistent with our expectation. In order to determine the eigenmode of the actual structure, we excite the sound source at the corresponding location (blue dots) and at the corresponding frequency (268, 408, 534, and 615 Hz), and measure the

sound field in all the cavities, as shown in Figs. 4(c)–4(f). Figures 4(c)–4(f) indicate that the measured sound fields match the simulation results in Figs. 3(c)–3(f).

According to Fig. 4(b), once the surface impedances are continuously distributed in a gradient at the boundaries, topologically protected broadband rainbow-trapping can be realized [37–39]. The ability of acoustic rainbow localized sound waves of different frequencies is shown under the excitation of a fixed sound source. We used 5×15 unit cells to design a nontrivial interface with the relationship between the lengths *l* and the positions of the outermost tubes as shown in Fig. 5(a). The sound source is placed in the cavity at site 1. We measure the acoustic energy of the cavity at the boundary at a frequency ranging from 275 to 295 Hz. The propagation of sound waves in the boundary lattice of different frequencies is shown in the Fig. 5(b). It can be seen that the propagation distance of sound waves of different frequencies is different. For example, we measure the sound field distribution of the entire structure at different frequencies (275, 285, and 295 Hz) as shown in Fig. 5(c). As we can see, the higher the frequency, the farther the sound waves travel. This allows the sound

waves of different frequencies to be separated, forming an acoustic rainbow.

Compared with other works on this topic, we directly change the group velocity of the edge state, operating only on the boundary without changing the bulk lattice. Most of the entire structure does not need to be changed when regulating rainbow-trapping. The rainbow-trapping occurs at the boundary of a nontrivial structure and does not require additional regions. Besides, our model is based on resonance rather than scattering, which facilitates the design of subwavelength structures. All parameters of the model can be calculated using acoustic parameters, which facilitates the design of structures given the expected working frequencies.

V. CONCLUSION

In conclusion, we propose that the frequency and group velocity of topological edge states can be controlled by the on-site potential, and realize broadband rainbow-trapping based on a prototype of an acoustic topological concentrator. We link the concepts in classical wave systems with condensed matter physics theory, and demonstrate that tuning the surface impedance of an acoustic topological insulator at the boundary is an effective way to control the topological state, which in the theoretical model corresponds to tuning on-site potential at the boundary. We obtain a rigorous mathematical relationship between the geometrical parameters of the structure and the Hamiltonian in the theoretical model, which helps to design a specific acoustic device more efficiently. Based on these considerations, topological rainbow-trapping is achieved. Topological properties of edge states make it robust compared to traditional methods, while the resonant nature of the structure makes subwavelength and broadband operation easier to achieve. We hope this work can be helpful for acoustic devices related to spatial modulation and provide a versatile platform for the design and application of topological materials.

ACKNOWLEDGMENTS

[1] M. Z. Hasan and C. L. Kane, Colloquium: Topological insulators, Rev. Mod. Phys. **82,** 3045 (2010).

[2] X.-L. Qi and S.-C. Zhang, Topological insulators and superconductors, Rev. Mod. Phys. **83,** 1057 (2011).

[3] R. Yu, W. Zhang, H.-J. Zhang, S.-C. Zhang, X. Dai, and Z. Fang, Quantized anomalous Hall effect in magnetic topological insulators, Science **329,** 61 (2010).

[4] B. A. Bernevig, T. L. Hughes, and S.-C. Zhang, Quantum spin Hall effect and topological phase transition in HgTe quantum wells, Science **314,** 1757 (2006).

[5] C. L. Kane and E. J. Mele, Z_2 Topological Order and the Quantum Spin Hall Effect, Phys. Rev. Lett. **95,** 146802 (2005).

[6] C. L. Kane and E. J. Mele, Quantum Spin Hall Effect in Graphene, Phys. Rev. Lett. **95,** 226801 (2005).

[7] L. Fu, Topological Crystalline Insulators, Phys. Rev. Lett. **106,** 106802 (2011).

[8] C. Fang, M. J. Gilbert, and B. A. Bernevig, Bulk topological invariants in noninteracting point group symmetric insulators, Phys. Rev. B **86,** 115112 (2012).

[9] R.-J. Slager, A. Mesaros, V. Juričić, and J. Zaanen, The space group classification of topological band-insulators, Nat. Phys. **9,** 98 (2013).

[10] W. A. Benalcazar, B. A. Bernevig, and T. L. Hughes, Quantized electric multipole insulators, Science **357,** 61 (2017).

[11] F. Schindler, A. M. Cook, M. G. Vergniory, Z. Wang, S. S. P. Parkin, B. A. Bernevig, and T. Neupert, Higher-order topological insulators, Sci. Adv. **4,** eaat0346 (2018).

[12] C. W. Peterson, T. Li, W. A. Benalcazar, T. L. Hughes, and G. Bahl, A fractional corner anomaly reveals higher-order topology, Science **368,** 1114 (2020).

[13] W. A. Benalcazar, B. A. Bernevig, and T. L. Hughes, Electric multipole moments, topological multipole moment pumping, and chiral hinge states in crystalline insulators, Phys. Rev. B **96,** 245115 (2017).

[14] W. A. Benalcazar, T. Li, and T. L. Hughes, Quantization of fractional corner charge in C_n-symmetric higher-order topological crystalline insulators, Phys. Rev. B **99,** 245151 (2019).

[15] L.-H. Wu and X. Hu, Scheme for Achieving a Topological Photonic Crystal by using Dielectric Material, Phys. Rev. Lett. **114,** 223901 (2015).

[16] M. Xiao, Z. Q. Zhang, and C. T. Chan, Surface Impedance and Bulk Band Geometric Phases in One-Dimensional Systems, Phys. Rev. X **4,** 021017 (2014).

[17] J. Noh, W. A. Benalcazar, S. Huang, M. J. Collins, K. P. Chen, T. L. Hughes, and M. C. Rechtsman, Topological protection of photonic mid-gap defect modes, Nat. Photonics **12,** 408 (2018).

[18] M. Li, D. Zhirihin, M. Gorlach, X. Ni, D. Filonov, A. Slobozhanyuk, A. Alù, and A. B. Khanikaev, Higher-order topological states in photonic kagome crystals with long-range interactions, Nat. Photonics **14,** 89 (2020).

[19] B.-Y. Xie, G.-X. Su, H.-F. Wang, H. Su, X.-P. Shen, P. Zhan, M.-H. Lu, Z.-L. Wang, and Y.-F. Chen, Visualization of Higher-Order Topological Insulating Phases in Two-Dimensional Dielectric Photonic Crystals, Phys. Rev. Lett. **122,** 233903 (2019).

[20] X.-D. Chen, W.-M. Deng, F.-L. Shi, F.-L. Zhao, M. Chen, and J.-W. Dong, Direct Observation of Corner States in Second-Order Topological Photonic Crystal Slabs, Phys. Rev. Lett. **122,** 233902 (2019).

[21] H. T. Teo, H. Xue, and B. Zhang, Topological phase transition induced by gain and loss in a photonic chern insulator, Phys. Rev. A. **105**, 053510 (2022).

[22] M. Serra-Garcia, V. Peri, R. Süsstrunk, O. R. Bilal, T. Larsen, L. G. Villanueva, and S. D. Huber, Observation of a phononic quadrupole topological insulator, Nature **555**, 342 (2018).

[23] H. Fan, B. Xia, L. Tong, S. Zheng, and D. Yu, Elastic Higher-Order Topological Insulator with Topologically Protected Corner States, Phys. Rev. Lett. **122**, 204301 (2019).

[24] C. W. Peterson, W. A. Benalcazar, T. L. Hughes, and G. Bahl, A quantized microwave quadrupole insulator with topologically protected corner states, Nature **555**, 346 (2018).

[25] S. Imhof, C. Berger, F. Bayer, J. Brehm, L. W. Molenkamp, T. Kiessling, F. Schindler, C. H. Lee, M. Greiter, T. Neupert, and R. Thomale, Topolectrical-circuit realization of topological corner modes, Nat. Phys. **14**, 925 (2018).

[26] F. Zangeneh-Nejad and R. Fleury, Nonlinear Second-Order Topological Insulators, Phys. Rev. Lett. **123**, 053902 (2019).

[27] Z. Yang, F. Gao, X. Shi, X. Lin, Z. Gao, Y. Chong, and B. Zhang, Topological Acoustics, Phys. Rev. Lett. **114**, 114301 (2015).

[28] G. Ma, M. Xiao, and C. T. Chan, Topological phases in acoustic and mechanical systems, Nat. Rev. Phys. **1**, 281 (2019).

[29] X. Zhang, H.-X. Wang, Z.-K. Lin, Y. Tian, B. Xie, M.-H. Lu, Y.-F. Chen, and J.-H. Jiang, Second-order topology and multidimensional topological transitions in sonic crystals, Nat. Phys. **15**, 582 (2019).

[30] Z.-Z. Yang, X. Li, Y.-Y. Peng, X.-Y. Zou, and J.-C. Cheng, Helical Higher-Order Topological States in an Acoustic Crystalline Insulator, Phys. Rev. Lett. **125**, 255502 (2020).

[31] X. Ni, M. Weiner, A. Alù, and A. B. Khanikaev, Observation of higher-order topological acoustic states protected by generalized chiral symmetry, Nat. Mater. **18**, 113 (2019).

[32] H. Xue, Y. Yang, F. Gao, Y. Chong, and B. Zhang, Acoustic higher-order topological insulator on a kagome lattice, Nat. Mater. **18**, 108 (2019).

[33] X. Zhang, X. Bi-Ye, H.-F. Wang, X. Xu, Y. Tian, J.-H. Jiang, M.-H. Lu, and Y.-F. Chen, Dimensional hierarchy of higher-order topology in three-dimensional sonic crystals, Nat. Commun. **10**, 5331 (2019).

[34] M. Weiner, X. Ni, M. Li, A. Alù, and A. B. Khanikaev, Demonstration of a third-order hierarchy of topological states in a three-dimensional acoustic metamaterial, Sci. Adv. **6**, eaay4166 (2020).

[35] A.-Y. Guan, Z.-Z. Yang, X.-Y. Zou, and J.-C. Cheng, Method to Derive the Hamiltonian of Acoustic Topological Crystalline Insulators, Phys. Rev. Appl. **15**, 064056 (2021).

[36] W. Zhu, H. Xue, J. Gong, Y. Chong, and B. Zhang, Time-periodic corner states from floquet higher-order topology, Nat. Commun. **13**, 1038 (2022).

[37] K. L. Tsakmakidis, A. D. Boardman, and O. Hess, "Trapped rainbow" storage of light in metamaterials, Nature **450**, 397 (2007).

[38] M. F. Yanik and S. Fan, Stopping Light All Optically, Phys. Rev. Lett. **92**, 083901 (2004).

[39] Q. Gan, Y. J. Ding, and F. J. Bartoli, "Rainbow" Trapping and Releasing at Telecommunication Wavelengths, Phys. Rev. Lett. **102**, 056801 (2009).

[40] V. N. Smolyaninova, I. I. Smolyaninov, A. V. Kildishev, and V. M. Shalaev, Experimental observation of the trapped rainbow, Appl. Phys. Lett. **96**, 211121 (2010).

[41] M. S. Jang and H. Atwater, Plasmonic Rainbow Trapping Structures for Light Localization and Spectrum Splitting, Phys. Rev. Lett. **107**, 207401 (2011).

[42] R. Yang, W. K. Zhu, and J. J. Li, Realization of "trapped rainbow" in 1D slab waveguide with surface dispersion engineering, Opt. Express **23**, 6326 (2015).

[43] K. Liu and S. He, Truly trapped rainbow by utilizing nonreciprocal waveguides, Sci. Rep. **6**, 30206 (2016).

[44] A. O. Montazeri, Y. Fang, P. Sarrafi, and N. P. Kherani, Rainbow-trapping by adiabatic tuning of intragroove plasmon coupling, Opt. Express **24**, 26745 (2016).

[45] Z. Hayran, H. Kurt, and K. Staliunas, Rainbow trapping in a chirped three-dimensional photonic crystal, Sci. Rep. **7**, 3046 (2017).

[46] Z. Tian and L. Yu, Rainbow trapping of ultrasonic guided waves in chirped phononic crystal plates, Sci. Rep. **7**, 40004 (2017).

[47] Z. Xu, J. Shi, R. J. Davis, X. Yin, and D. F. Sievenpiper, Rainbow Trapping with Long Oscillation Lifetimes in Gradient Magnetoinductive Metasurfaces, Phys. Rev. Appl. **12**, 024043 (2019).

[48] J. Zhu, Y. Chen, X. Zhu, F. J. Garcia-Vidal, X. Yin, W. Zhang, and X. Zhang, Acoustic rainbow trapping, Sci. Rep. **3**, 1728 (2013).

[49] X. Ni, Y. Wu, Z.-G. Chen, L.-Y. Zheng, Y.-L. Xu, P. Nayar, X.-P. Liu, M.-H. Lu, and Y.-F. Chen, Acoustic rainbow trapping by coiling up space, Sci. Rep. **4**, 7038 (2015).

[50] A. Colombi, D. Colquitt, P. Roux, S. Guenneau, and R. V. Craster, A seismic metamaterial: The resonant metawedge, Sci. Rep. **6**, 27717 (2016).

[51] D. Cardella, P. Celli, and S. Gonella, Manipulating waves by distilling frequencies: A tunable shunt-enabled rainbow trap, Smart Mater. Struct. **25**, 085017 (2016).

[52] E. A. Skelton, R. V. Craster, A. Colombi, and D. J. Colquitt, The multi-physics metawedge: Graded arrays on fluid-loaded elastic plates and the mechanical analogues of rainbow trapping and mode conversion, New J. Phys. **20**, 053017 (2018).

[53] A. Arreola-Lucas, G. Báez, F. Cervera, A. Climente, R. A. Méndez-Sánchez, and J. Sánchez-Dehesa, Experimental evidence of rainbow trapping and Bloch oscillations of torsional waves in chirped metallic beams, Sci. Rep. **9**, 1860 (2019).

[54] H. Meng, N. Bailey, Y. Chen, L. Wang, F. Ciampa, A. Fabro, D. Chronopoulos, and W. Elmadih, 3D rainbow phononic crystals for extended vibration attenuation bands, Sci. Rep. **10**, 18989 (2020).

[55] J. M. De Ponti, L. Iorio, E. Riva, R. Ardito, F. Braghin, and A. Corigliano, Selective Mode Conversion and Rainbow Trapping via Graded Elastic Waveguides, Phys. Rev. Appl. **16**, 034028 (2021).

[56] M. Alshaqaq, C. Sugino, and A. Erturk, Programmable Rainbow Trapping and Band-Gap Enhancement via Spatial Group-Velocity Tailoring in Elastic Metamaterials, Phys. Rev. Appl. **17**, L021003 (2022).

[57] J. Guglielmon and M. C. Rechtsman, Broadband Topological Slow Light Through Higher Momentum-Space Winding, Phys. Rev. Lett. **122**, 153904 (2019).

[58] G. J. Chaplain, J. M. De Ponti, G. Aguzzi, A. Colombi, and R. V. Craster, Topological Rainbow Trapping for Elastic Energy Harvesting in Graded Su-Schrieffer-Heeger Systems, Phys. Rev. Appl. **14**, 054035 (2020).

[59] C. Lu, C. Wang, M. Xiao, Z. Q. Zhang, and C. T. Chan, Topological Rainbow Concentrator Based on Synthetic Dimension, Phys. Rev. Lett. **126**, 113902 (2021).

[60] B. Ungureanu, M. P. Makwana, R. V. Craster, and S. Guenneau, Localizing Elastic Edge Waves via the Topological Rainbow Effect, Phys. Rev. Appl. **15**, 014057 (2021).

[61] L. Yu, H. Xue, B. Zhang, and Topological slow light via coupling chiral edge modes with flatbands, Topological slow light via coupling chiral edge modes with flatbands, Appl. Phys. Lett. **118**, 071102 (2021).

[62] Z. Wang, Z. Wang, H. Li, Z. Liu, J. Luo, F. Huang, J. Huang, X. Wang, H. Li, and H. Yang, Probing Two Distinct Types of Topological Rainbow Concentrators Related to the Acoustic Valley Hall Insulator in Synthesized Three-Dimensional Space, Phys. Rev. Appl. **17**, 064002 (2022).

[63] See Supplemental Material at http://link.aps.org/supplemental/10.1103/PhysRevApplied.18.044054, which includes tight-binding model of the 2D SSH model in classical wave systems, impact of surface impedance on topological states in classical wave systems, coupling oscillation in higher-order topological insulators, details of the prototype of topological rainbow-trapping, energy shifts of corner-localized states in topological crystalline insulators with a C_3- or C_6-symmetric lattice, rainbow-trapping in 3D higher-order topological insulators, and details of the experimental configuration.

[64] F. Liu and K. Wakabayashi, Novel Topological Phase with a Zero Berry Curvature, Phys. Rev. Lett. **118**, 076803 (2017).

[65] F. Liu, H.-Y. Deng, and K. Wakabayashi, Helical Topological Edge States in a Quadrupole Phase, Phys. Rev. Lett. **122**, 086804 (2019).